Bio-based design and synthesis of lignin-*graft*-lignin copolymers and their nanomaterials

Tingting Wu[a,1], Sigit Sugiarto[a,1], Pei Lin Chee[b], Chen-Gang Wang[a], Pin Jin Ong[b], Ruochen Yang[a], Gaodan Liu[b,c], Qiang Zhu[b], Zibiao Li[a,b], Xian Jun Loh[b,*], Dan Kai[a,b,*]

[a]Institute of Sustainability for Chemicals, Energy and Environment (ISCE^2), Agency for Science, Technology and Research (A*STAR), 1 Pesek Road, Jurong Island 627833, Singapore

[b]Institute of Materials Research and Engineering (IMRE), Agency for Science, Technology and Research (A*STAR), 2 Fusionopolis Way, Innovis #08-03, 138634, Singapore

[c]Department of Food Science and Engineering, Zhejiang University of Technology, Hangzhou, 310014, P. R. China

Corresponding author: lohxj@imre.a-star.edu.sg; kaid@imre.a-star.edu.sg

[1]Tingting Wu and Sigit Sugiarto contributed equally to this article.

Abstract: Lignin, the most abundant natural aromatic biopolymer, is a promising alternative to petroleum-based polymers. Extensive efforts have been devoted to its chemical modifications for high-value applications, with lignin-grafted copolymer nanomaterials emerging as a key advancement. However, the relationships between copolymerization and nanomaterial properties of lignin are rarely studied. Here, we copolymerized three lignin derivative monomers (FMA, VMA, and SMA) onto lignin via reversible addition-fragmentation chain transfer (RAFT) copolymerization and investigated how these lignin copolymers improve the functionality and processability of lignin and affect the properties of resulting lignin nanomaterials. The successful copolymerization was verified by NMR and GPC. The grafting kinetics were revealed, with FMA exhibiting the highest reactivity, followed by VMA and SMA. Lignin-copolymer nanobeads were prepared via a solvent-shifting process, showing spherical shapes with diameters of 152 nm for Lignin-PFMA, 125 nm for Lignin-PVMA, and 176 nm for Lignin-PSMA, respectively. The lignin nanofibers are also obtained by electrospinning without the assistance of other synthetic polymers with fiber diameters ranging from 310 to 1180 nm. The cell viability attained from the incubation of lignin nanobeads and nanofibers for either CCL9.1 or WS1 cells was above 80%, which indicates their good biocompatibility. Together their unique antioxidant and UV-absorbing properties, the lignin nanomaterials demonstrate great potential for biomedical applications, including UV-protective pharmaceutical formulations and antioxidative biomaterials for wound healing / tissue engineering.

Keywords: Lignin derivatives, vanillin, RAFT polymerization, nanofibers, nanobeads, biomaterials

1. Introduction

Lignin is the primary source of natural aromatic polymers and the second most abundant renewable and sustainable biomass resource after cellulose (around 15-30% of whole lignocellulosic biomass) [1]. Lignin is the main byproduct of the global pulping industry and is the least utilized biomass component. Because of its unique chemical structures and properties, such as antioxidant, antibacterial, anti-UV, and good biocompatibility, it is a promising substitute for petroleum-based polymers [2-4]. However, its intrinsic recalcitrance, heterogeneity, and structural complexity strictly limited its wide applications, especially in the development of lignin-based functional and high-performance materials.

Due to such limitations, most studies focus on developing lignin-based nanoparticles, which can be easily fabricated via self-assembly. Lignin self-assemblies into nanobeads/nanoparticles are mainly driven by the solvent-lignin-antisolvent interactions, which are prepared through a solvent-shifting method via dialysis [5]. Lignin-engineered nanobeads/nanoparticles have been widely investigated as reinforcing agents [6] in nanocomposites and carriers for biologically active substances, such as drug delivery [7]. Moreover, a significant number of studies have chemically modified lignin with other common polymers through grafting, such as poly (lactic acid) (PLA) [8, 9], poly(ε-caprolactone) (PCL) [10, 11], and polyhydroxybutyrate (PHB) [12], to make it feasible for electrospinning to realize nanofibrous mats for biomedical applications.

The richness of functional phenolic and aliphatic hydroxyl groups endows lignin with great potential for chemical modification [13]. The polymerization of lignin is considered a method to overcome its limitations and shows potential for converting lignin into functional and high-performance polymeric materials. Grafting copolymerization involves attaching polymer chains to the hydroxyl groups on the lignin structure, resulting in lignins with star-like branched copolymers [14]. Numerous researchers have exploited the reversible addition-fragmentation chain transfer (RAFT) polymerization and atom transfer radical polymerization (ATRP) of lignin to broaden its application scenarios and increase its adoption volumes [14]. In those works, monomers/polymers used in ATRP or RAFT polymerization to graft in lignins

are petroleum-based, such as poly(ethylene glycol) methyl ether methacrylate [15], glycidyl methacrylate [16], and N-isopropylacrylamide [17]. It is meaningful to explore new, sustainable, and biodegradable biomass-based grafting monomers to replace conventional petroleum-derived alternatives. In this study, we use lignin-derived monomers for lignin grafting to get a series of lignin-*graft*-lignin copolymers via RAFT copolymerization.

The copolymerization of lignin brings promising opportunities for the development of high-value lignin-derived nanomaterials with tailored morphology and properties. However, the relationship between lignin copolymers and the resulting nanomaterials, such as the above-mentioned nanobeads and nanofibers, is unclear. Currently, there is a lack of comprehensive studies delving into the relationship between the structural features of lignin-based grafted copolymers and the key properties of obtained nanomaterials, such as the capability for electrospinning, the fiber diameters, the morphology and stability of nanobeads/nanoparticles, and even their biocompatibility through cytotoxicity. Therefore, figuring out the relationship between the chemical structure of lignin-based copolymers and the processing and properties of the obtained nanomaterials could potentially instruct the future design and realization of new lignin-based nanomaterials.

In this work, three kinds of lignin derivative monomers (4-formylphenyl methacrylate (FMA), vanillin methacrylate (VMA), and syringaldehyde methacrylate (SMA)) were synthesized and grafted onto lignin to achieve functional lignin copolymers. These grafted copolymers have chemical structural similarities to lignin. Therefore, graft copolymerization of lignin with these derivatives could potentially enhance both the functionality and processability of lignin-based copolymers, enabling the production of nanofibers without the need for other synthetic polymers. Exploring the subtle structural disparities among these three monomers could yield deeper insights into the intricacies of the lignin copolymerization mechanism, facilitating a deeper comparative analysis of the resultant lignin nanomaterials. These lignin copolymers were fabricated into nanobeads and nanofibers to reveal the properties of lignin-based copolymers. The biocompatibility of obtained nanobeads and nanofibers was characterized by cell viability. The lignin modification and subsequent engineering process into nanobeads and nanofibers are shown in **Scheme 1**.

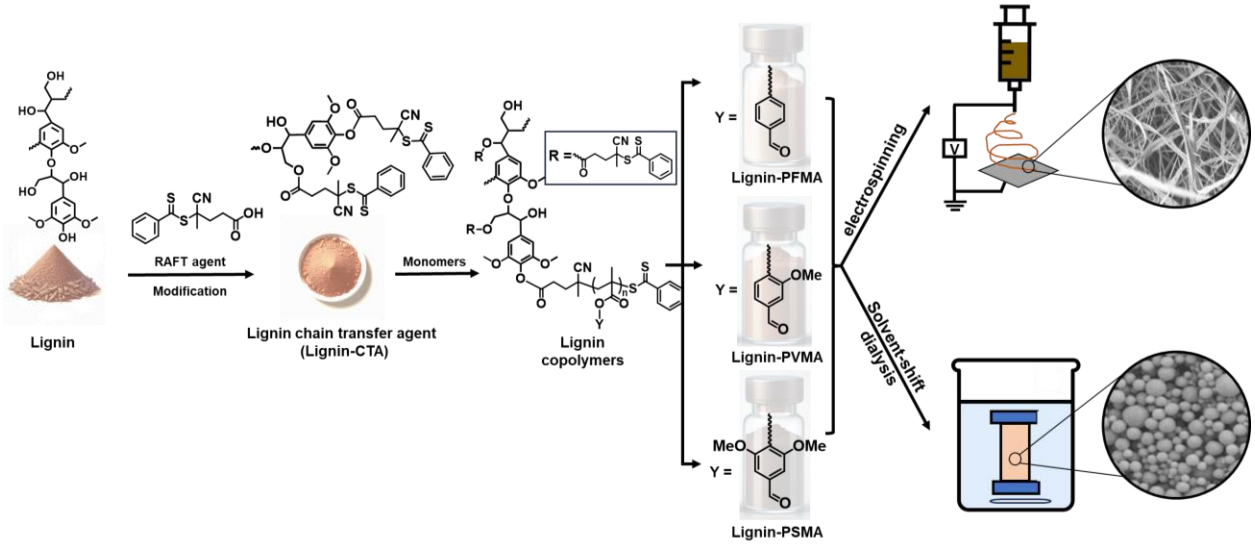

Scheme 1. Scheme of the lignin copolymerization and subsequent engineering process into nanofibers and nanobeads.

2. Materials and methods

2.1. Materials

Lignin, tetrahydrofuran (THF), 1,1,1,3,3,3-hexafluoro-2-propanol (HFP), dimethylformamide (DMF), dichloromethane (DCM), chloroform ($CHCl_3$), sodium hydroxide (NaOH), hydrogen chloride (HCl), methacrylic anhydride (MAA), and ethyl acetate were purchased from Sigma Aldrich. Hexane and diethyl ether were sourced from Fischer Scientific. Magnesium sulfate ($MgSO_4$) and methanol were acquired from Kanto Chemical, and ethanol was sourced from VWR Chemicals. The RAFT agent (4-vyano-4-(phenylcarbonothioylthio)pentanoic acid, 97%) was obtained from Strem. N, N'-Dicyclohexylcarbodiimide (DCC), vanillin, 4-dimethylaminopyridine (DMAP), azobisisobutyronitrile (AIBN), 4-hydroxybenzaldehyde, trimethylamine, and methacryloyl chloride were obtained from Sigma Aldrich. All the chemicals are used as obtained. CCL9.1 is an epithelial-like cell that was isolated from the liver of a male mouse. WS1 is a fibroblast cell isolated from the skin of a black female donor. Both CCL9.1 and WS1 cells were obtained from ATCC, USA.

2.2. Synthesis and preparation

2.2.1. Synthesis of lignin chain transfer agent (lignin-CTA)

Lignin (5 g), 4-vyano-4-(phenylcarbonothioylthio)pentanoic acid (RAFT agent, 3.33 g), 4-dimethylaminopyridine (DMAP, 1.613 g), and anhydrous DMF (20 mL) were added to a 50 mL round-bottom flask with magnetic stirring. N,N'-Dicyclohexylcarbodiimide (DCC, 3.096 g) and DMF (dry, 5 mL) were mixed and added dropwise into the round-bottom flask under N_2. The reaction was kept at room temperature for 24 h under N_2. Upon completion, the product was centrifuged to remove the solid side product and purified by precipitation twice using diethyl ether/ethanol (V/V= 1/1, 500 mL). The solution was centrifuged to collect the solid. The product was dried under vacuum to yield lignin-CTA (4.83 g, 67% yield, 1.59 mmol RAFT agent/g) as a brown powder.

2.2.2. Synthesis of monomers: FMA, VMA, and SMA

4-Hydroxybenzaldehyde (10.0 g, 81.9 mmol), trimethylamine (9.11 g, 90.0 mmol), and THF (80 mL) were placed in a round-bottom flask with a stir bar. After stirring for 5 min, methacryloyl chloride (9.41 g, 90 mmol) was added to the reaction mixture dropwise at 0 °C. The reaction temperature was raised to room temperature and kept at room temperature for 8 h. After the reaction, the reaction mixture was filtered to remove insoluble salts, and the solution was diluted with DI water (100 mL). The solution was extracted with DCM (60 mL) three times, and the organic layer was dried over $MgSO_4$ and evaporated. The crude was purified by column chromatography (eluent: hexane/ethyl acetate = 5/1 (V/V)). The product solution was evaporated and dried under vacuum to give 4-formylphenyl methacrylate (**FMA**, 13.72 g, 88% yield) as a white powder. Vanillin (30.43 g, 0.2 mol), 4-dimethylaminopyridine (DMAP, 0.17 g, 0.0014 mol), and methacrylic anhydride (MAA, 33.92 g, 0.22 mol) were added to a 250 mL round-bottom flask with a stir bar. The reaction temperature was raised to 60 °C, and the reaction was allowed to last for 24 h. After the reaction, the flask was cooled to room temperature, and the product was diluted with 150 mL of DCM. The resulting solution was then transferred to a separatory funnel and sequentially washed with 150 mL of 1.0 M NaOH, followed by 0.5 M NaOH, 1.0 M HCl, and finally, water. The organic phase was then dried over magnesium sulfate ($MgSO_4$) and concentrated using rotary evaporation. The crude was further purified by

column chromatography (eluent: hexane/ethyl acetate = 5/1 (V/V)). The product solution was evaporated and dried under vacuum to give vanillin methacrylate (**VMA**, 39.6 g, 90% yield) as a white powder. Syringaldehyde (10 g, 0.2 mol), 4-dimethylaminopyridine (DMAP, 1.613 g, 0.066 mol), methacrylic anhydride (MAA, 9.3087 g, 0.22 mol), and anhydrous THF (30 mL) were added to a 100 mL round-bottom flask with a magnetic stir bar. The reaction temperature was raised to 60 °C, and the reaction was allowed to last for 24 h. After the reaction, the flask was cooled to room temperature, and the product was diluted with 150 mL of DCM. The resulting solution was then transferred to a separatory funnel and sequentially washed with 150 mL of 1.0 M NaOH, followed by 0.5 M NaOH, 1.0 M HCl, and finally, water. The organic phase was then dried over magnesium sulfate ($MgSO_4$) and concentrated using rotary evaporation. The product was dried under vacuum to give syringaldehyde methacrylate (**SMA**, 12.4112 g, 90% yield) as a white powder.

2.2.3. Synthesis of copolymers: Lignin-PFMA, Lignin-PVMA, and Lignin-PSMA

Lignin-CTA (0.02 g, 0.032 mol RAFT agent), 4-formylphenyl methacrylate (FMA, 0.175 g, 100 mol), azobisisobutyronitrile (AIBN, 0.302 mg, 0.2 mol), and THF (90 wt% of solution) were mixed in a Schlenk flask and bubbled with N_2 for 5 min. The solution was stirred at 70 °C for 6 h. After 6 h, the solution was cooled to room temperature and precipitated with hexane/ethanol (V/V = 1/1, 200 mL). The solution was centrifuged, and the solid was collected and dried under vacuum to yield **Lignin-PFMA** polymer (0.10 g, 52% yield, FMA conversion = 62%) as a brown powder. Lignin-CTA (0.1 g, 0.159 mol RAFT agent), vanillin methacrylate (VMA, 1.012 g, 100 mol), azobisisobutyronitrile (AIBN, 1.51 mg, 0.2 mol), and THF (90 wt% of solution) were mixed in a Schlenk flask and bubbled with N_2 for 5 min. The solution was stirred at 70 °C for 16 h. After 16 h, the solution was cooled to room temperature and precipitated with methanol (200 mL). The solution was filtered, and the solid was collected and dried under vacuum to yield **Lignin-PVMA** polymer (0.59 g, 52.7% yield, VMA conversion = 54%) as a brown powder. Lignin-CTA (0.1 g, 0.159 mol RAFT agent), syringaldehyde methacrylate (SMA, 1.15 g, 100 mol), azobisisobutyronitrile (AIBN, 1.51 mg, 0.2 mol), and THF (90 wt% of solution) were mixed in a Schlenk flask and bubbled with

N_2 for 5 min. The solution was stirred at 70 °C for 10 h. After 10 h, the solution was cooled to room temperature and precipitated with methanol (200 mL). The solution was centrifuged, and the solid was collected and dried under vacuum to yield **Lignin-PSMA** polymer (0.23 g, 19.1% yield, SMA conversion = 30%) as a brown powder.

2.2.4. Lignin nanobeads via dialysis

Lignin copolymers were dissolved in THF at 1 mg/mL. The solution was filtered through a 0.2 μm polytetrafluoroethylene (PTFE) syringe filter. All lignin copolymers are not 100% soluble in THF. Lignin-PSMA has the best solubility, Lignin-PVMA has moderate solubility, and Lignin-PFMA has the least solubility in THF. The filtered solution was dialyzed (cut-off 3.5 kD) in DI water for 24 h and freeze-dried for characterization. For the Sigma lignin reference sample, the lignin purchased from Sigma was dissolved in methanol at 1 mg/mL, and the following dialysis procedure was kept the same.

2.2.5. Lignin nanofibers via electrospinning

Lignin polymers were dissolved in 1,1,1,3,3,3-hexafluoro-2-propanol (HFP) to prepare electrospinning solutions. Specifically, solutions of 12 wt% Lignin-PSMA and Lignin-PFMA were prepared for electrospinning, while a concentration of 10 wt% was used for Lignin-PVMA due to challenges encountered during dissolution in HFP, resulting in gel-like lumps. A 3 mL syringe fitted with a 22-gauge flat-tipped needle was used for the dispensation of the solution. The syringe was placed on a syringe pump with a controlled rate of 1 mL/min. Electrospinning was carried out using an applied voltage of 12 kV, with the needle tip-to-collector distance set at 10 cm to ensure optimal nanofiber formation.

2.3. Characterization

2.3.1. Nuclear magnetic resonance (NMR)

The chemical structures of synthesized monomer, lignin-CTA, and lignin copolymers were characterized using a JEOL 400 MHz NMR spectrometer for ^{1}H NMR analysis. Approximately 10-20 mg of the synthesized monomer, lignin-CTA, and lignin copolymers were dissolved in deuterated chloroform

($CDCl_3$). Quantitative analysis of lignin-CTA was carried out by NMR with $CHCl_3$ as an external standard. For this analysis, 2.49 mg of $CHCl_3$ was used alongside 3.54 mg of lignin-CTA.

2.3.2. Gel permeation chromatography (GPC)

The molecular weights and polydispersity indices (PDI) of lignin-CTA and lignin copolymers were measured by gel permeation chromatography (GPC) using a Shimadzu system (SIL-20A prominence, LC-20AD prominence, RID-10A, CTO-10A, Shimadzu Co., Kyoto, Japan). The analysis was performed with THF as the eluent, utilizing GPC columns (Shodex GPC KF-804, Shimadzu Co., Kyoto, Japan) at a flow rate of 1.0 mL/min and a temperature of 25 °C. The number-average molecular weights (Mn), weight-average molecular weights (Mw), and PDI (Mw/Mn) were calculated based on calibration with linear polystyrene standards. Samples of lignin-CTA and lignin copolymers were prepared at 1 mg/mL in HPLC-grade THF, followed by filtration through a 0.2 μm PTFE syringe filter.

2.3.3. Thermogravimetric Analysis (TGA) and Differential Scanning Calorimetry (DSC)

The thermal stability of lignin copolymers was assessed using a thermogravimetric analyzer (TGA Q500, TA Instruments). The lignin copolymers underwent heating up to 700 °C at a rate of 20 °C/min under a nitrogen flow of 60 mL/min. For the differential scanning calorimeter (DSC) thermal analysis, lignin copolymers were analyzed using a DSC3 STARe System (Mettler Toledo) equipped with an auto-cool accessory and calibrated with indium. The samples underwent a specific temperature ramp of 10 °C/min: heated from -60 °C to 180 °C and held in isotherm for 5 min to complete the first heating cycle to remove thermal history. Subsequently, the samples were cooled from 180 °C to -60 °C, held for 5 min, and then reheated from -60 °C to 180 °C to complete the second heating cycle. Glass transition temperature (T_g) was determined in the second heating cycle for all samples.

2.3.4. Scanning electrode microscope (SEM)

The morphology and microstructure of the electrospun lignin-engineered nanofibers were characterized using a scanning electron microscope (JSM6700F, JEOL, Japan). Prior to imaging, the samples were

mounted onto the stage using double-sided carbon tape and sputter-coated with a thin layer of gold using a sputter fine coater (JFC-1200, JEOL, Japan) to enhance surface conductivity. The SEM analysis was performed at an accelerating voltage of 5 kV, with a working distance of 8 mm. Multiple randomly selected regions across the sample were examined to ensure the representation of the entire sample. Next, we measured the diameter of the lignin nanofibers by taking readings from 50 random spots using Image J software (National Institutes of Health in Bethesda, USA).

2.3.5. Transmission electron microscopy (TEM)

Transmission Electron Microscopy (TEM) was used to investigate the morphology and dimensions of lignin nanomaterial samples. A 10 μL aliquot of a 0.01 wt% nanolignin dispersion was carefully drop-cast onto a glow-discharged carbon-coated copper (Cu) grid, allowing it to naturally dry via evaporation. Subsequently, the samples underwent observation via a TEM microscope operating at 200 kV (FEI Titan 80-300 kV TEM). To measure the diameter of lignin nanobeads, we conducted measurements on at least 50 random locations using Image J.

2.3.6. Water contact angle

The water contact angle of the nanofiber samples was determined using the VCA Optima Surface Analysis System (AST Products, Billerica, MA, USA). Nanofiber samples were securely placed on glass slides, ensuring minimal wrinkles or folds. 7.5 μL of deionized water was carefully dispensed onto the sample surface using an injection syringe. The contact between the water droplet and the nanofiber sample was recorded with a high-resolution camera, and multiple images were captured for accurate angle measurement. Image analysis software provided with the VCA Optima System was utilized to measure the contact angle between the tangent to the droplet interface and the solid surface of the nanofiber sample. Multiple measurements were taken at different locations on each sample to account for surface heterogeneity, and the average contact angle value was calculated for analysis.

2.3.7. Dynamic light scattering (DLS)

The size and zeta potential of lignin and lignin nanobeads were assessed with the aid of Malvern Zetasizer, NANO ZS (Malvern Instruments Limited, U.K.). The measurement was recorded for 0.2 mg/ml lignin nanobeads and 0.31mg/mL sigma-lignin-EG. The stability test was performed across 112 days at 25 °C.

2.3.8. Optical microscope and UV-Vis spectroscopy

The morphology of lignin nanobeads after the cell viability test was observed using an inverted optical microscope (Leica DMi8). The UV-Vis spectra of lignin copolymers were measured using a Cary 5000 UV-Vis-NIR Spectrophotometer (Agilent Co., USA). A quartz cell with a path length of 10 mm was used for measurements, and a baseline calibration was conducted using blank dimethylformamide (DMF). Lignin-PFMA and Lignin-PSMA were dissolved in DMF at 0.1 mg/mL, while Lignin-PVMA was prepared at 0.2 mg/mL due to its lower solubility. All solutions were filtered using a 0.22 μm PTFE syringe filter prior to measurement. Two cream formulations, with and without lignin nanoparticles, were applied to quartz vials and analyzed using UV-Vis spectroscopy.

2.3.9. Antioxidant assay

The antioxidant activity of lignin copolymers was evaluated using the 1,1-diphenyl-2-picrylhydrazyl (DPPH) radical scavenging assay modified from established protocols [18, 19]. Briefly, lignin copolymers (10 mg) were incubated with 10 mL of a 60 μM methanolic DPPH solution in glass vials at room temperature. The reduction of DPPH free radicals was monitored by measuring absorbance at 517 nm at regular intervals. All experiments were performed in triplicate. Antioxidant activity was expressed as the percentage of DPPH inhibition relative to control solutions, calculated as:

$$\% \text{ Inhibition} = \left(1 - \frac{\mathrm{A}_{sample}}{\mathrm{A}_{control}}\right) \times 100$$

where A_{sample} and $A_{control}$ represent the absorbance of the sample and control (DPPH solution without any copolymer), respectively.

2.4. Cell viability test

The lignin nanobead suspensions were prepared in phosphate-buffered saline. WS1 cells were cultured in Dulbecco's modified Eagle's medium (DMEM) supplemented with 10% fetal bovine serum and 1% penicillin streptomycin. CCL9.1 cells were cultured in DMEM supplemented with 10% horse serum. The cells were seeded in 96-well plates at a density of 5000 cells per well and incubated overnight at 37 °C with 5% carbon dioxide. 100 µL nanobead suspension was added into each well and incubated for another night. Three lignin nanobead concentrations were tested, which included 0.2 mg/mL, 0.1 mg/mL, and 0.05 mg/mL. Similarly, the lignin nanofibers were left to soak in the phosphate-buffered solution overnight before 5000 cells were seeded into each well. The cell viability test was assessed using the cell titer blue assay. Cytotoxicity tests were conducted on day 3 after the cells were seeded. The dye was added to the wells, and the plates were incubated at 37 °C for 4 h. The measurement was recorded with a microplate reader (Infinite M200, Tecan) at the excitation wavelength and emission wavelength of 560 nm and 590 nm, respectively. The wells with cells only served as the positive controls, whereas the negative control used was those containing 1% sodium lauryl sulfate. All the experiment was carried out in triplicate.

2.5. Statistical analysis

All data were displayed as mean ± standard deviation. Statistical analysis was performed using Student's t-test and one-way ANOVA, with differences between groups considered statistically significant at $p < 0.05$.

3. Results and Discussions

3.1. CTA functionalization of lignin and its copolymerization with vanillin derivatives

The synthesis route for the modification of lignin is outlined in **Figure 1a**, providing a visual representation of the sequential steps involved in the grafting process. The lignin chain transfer agent (lignin-CTA) was functionalized with 4-Cyano-4-(phenylcarbonothioylthio)pentanoic acid as the RAFT (Reversible Addition Fragmentation Chain Transfer) agent. Quantitative NMR analysis on the dithioester moiety indicated a grafting density of approximately 0.46 mmol of RAFT groups per gram of lignin (**Figure S1**). The calculation, using $CHCl_3$ as the external standard, has been included in the supporting information

(Figure S1). The molecular weight of the lignin-CTA was 5,200 g/mol as determined by GPC with THF as eluent. Previous work on lignin copolymerization via RAFT reported that the molecular weight of the original lignin was 3429 [20]. The schematic elucidates the key stages, including the initiation of RAFT polymerization using AIBN as a radical source, the incorporation of FMA, VMA, or SMA monomers, and the formation of lignin copolymers. The synthetic processes of three monomers, FMA, VMA, and SMA, are shown in **Figure S2,** and the NMR spectra of the respective monomers are presented in **Figure S3**. The successful synthesis of lignin copolymers via RAFT polymerization was validated using ^{1}H NMR analysis, which provided structural information. The grafting of FMA, VMA, and SMA monomers into the lignin backbone was confirmed through characteristic chemical shifts observed in the spectra (Figure 1b). Notably, the appearance of a peak at around 10 ppm (labeled k) in the NMR spectra of Lignin-PFMA indicated the presence of aldehyde protons, which was absent in the spectra of lignin-CTA. In comparison, the pronounced broad peaks at around 7-8 ppm (labeled i and j) were attributed to the phenyl protons on the PFMA grafted onto lignin. In addition, the absence of the alkene protons signals of the methacrylate group of the FMA monomer further provided further evidence of successful grafting of FMA onto lignin-CTA. The NMR spectra for Lignin-PVMA and Lignin-PSMA were presented in **Figure S4** and **S5**, respectively. However, it is also worth noting that a higher AIBN-to-RAFT agent ratio (0.2 mol AIBN to 0.032 mol RAFT agent) was employed to ensure a sufficient polymerization rate, particularly given the steric complexity of lignin, which can hinder radical diffusion. While an excess of AIBN may have contributed to the formation of some free, non-grafted polymer chains, the NMR and GPC analysis confirmed that successful RAFT-mediated grafting onto lignin occurred. In addition, the substantial increase in molecular weight (from 5,200 to ~15,000-20,000 g/mol), along with monomer-dependent differences in hydrodynamic radius (e.g., PVMA's compact high-Mw structure) and solubility, further confirms the dominance of grafted copolymers over free polymer chains in the final product. Future studies could optimize the initiator-to-RAFT-agent molar ratio (e.g. reducing AIBN:RAFT agent from 6:1 to 2:1) or employ selective precipitation to minimize free polymer formation. While the current ratio ensured efficient

polymerization despite lignin's steric constraints, the dominance of grafted copolymers is supported by the molecular weight increase, solubility differences, and particle size trends.

The kinetics study revealed expected differences in the reactivity of the monomers, with FMA exhibiting the highest reactivity, followed by VMA and SMA (Figure 1c). The observed differences in reaction kinetics among the monomers FMA, VMA, and SMA can be rationalized by considering factors such as steric hindrance and electron-withdrawing effects [21, 22]. Firstly, FMA, lacking methoxy groups on the ortho positions, experiences less steric hindrance during the polymerization reaction, facilitating faster access to lignin-CTA compared to VMA and SMA. In addition, a kinetics study by Chung et al. showed that in ATRP polymerization of lignin with styrene, the extended branching hinders monomer accessibility to active species, contributing to deviations from ideal living polymerization behavior [23]. Understanding the effects of hindrance effects from monomer structure and polymer branching highlights key kinetics in lignin. This study further explained the observed deviation from true first-order kinetics behavior, which is typical in controlled radical polymerizations, such as RAFT polymerization. Secondly, the presence of methoxy groups in VMA and SMA induces electron-withdrawing effects on the aromatic ring, reducing the electron density and thereby diminishing the reactivity of the monomers in comparison to FMA. These factors collectively influence the rate of grafting onto lignin, highlighting the intricate interplay between monomer structure and reactivity in RAFT polymerization processes.

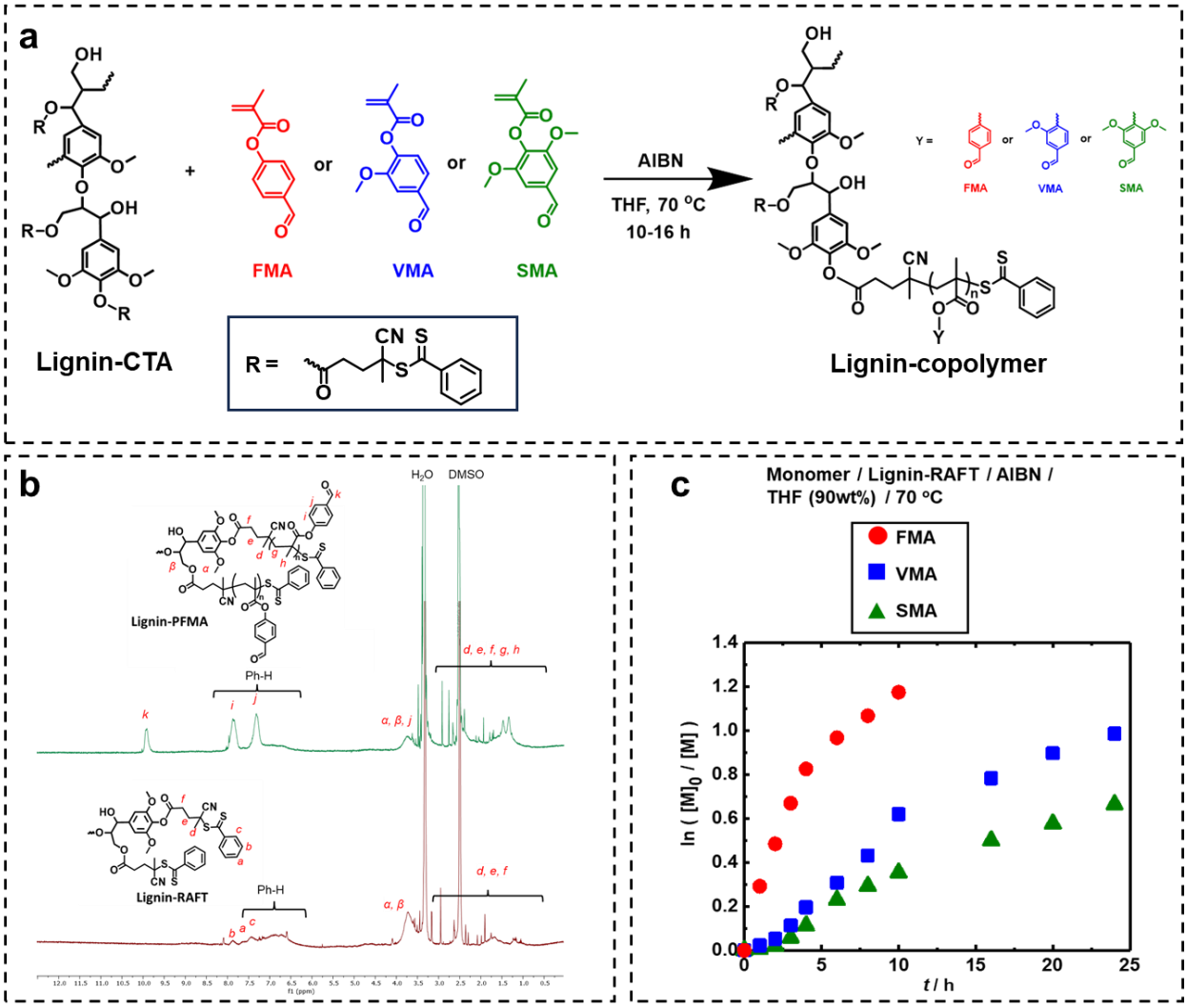

Figure 1. (a) Schematics showing the grafting process of FMA, VMA, and SMA onto lignin-CTA. (b) An example of NMR spectra of Lignin-PFMA copolymer and lignin-CTA. (c) A kinetic study conducted to examine the chemical modification process of lignin.

The thermal stability of the obtained lignin-based copolymers was evaluated through thermogravimetric analysis (TGA) under a nitrogen atmosphere. As shown in **Figure 2a**, Lignin-PVMA and Lignin-PSMA show very similar thermal degradation behavior, with T_{d5} of 214.3 °C and 225.9 °C and T_{d10} of 254.8 °C and 260.8 °C, respectively. However, from the DTG curve, a small peak around 200 °C was observed for Lignin-PFMA, leading to a T_{d5} of 191.1 °C and T_{d10} of 217.1 °C. This early thermal degradation could be attributed to the low stability of grafted FMA side groups in lignin-based copolymers.

The weight residues at 500 °C are 25.5 wt%, 31.3 wt%, and 38.0 wt% for Lignin-PFMA, Lignin-PVMA, and Lignin-PSMA, respectively (Table 1). The lignin core shows better thermal performance compared to the side grafting polymers; thus, the higher weight residues at 500 °C indicate higher weight ratios of lignin, that is, lower weight ratios of grafting polymers due to the higher steric hindrance of SMA monomers.

As shown in Figure 2b, the T_g (glass transition temperature) obtained from the endothermic stepwise change in differential scanning calorimetry (DSC) curves, taken using the DSC test software, are 110.9 °C and 126.2 °C for Lignin-PFMA and Lignin-PVMA, respectively. The absence of a clear T_g peak for Lignin-PSMA could be attributed to its low grafting ratio, which may result in insufficient signal strength or broadening of the transition, making it difficult to observe a distinct peak. Additionally, the chemical structure differences between PFMA, PVMA, and PSMA groups can significantly influence the thermal properties. The increased steric hindrance from the additional methyl groups in PSMA likely results in a higher T_g that may exceed the temperature range tested in the DSC experiment. Polymers with a higher T_g are generally more thermally stable and resistant to thermal deformation. This observation aligns with the TGA results. The obtained lignin-based copolymers present similar molecular weights, 18,000 g/mol for Lignin-PFMA, 19,000 g/mol for Lignin-PVMA, and 16,000 g/mol for Lignin-PSMA.

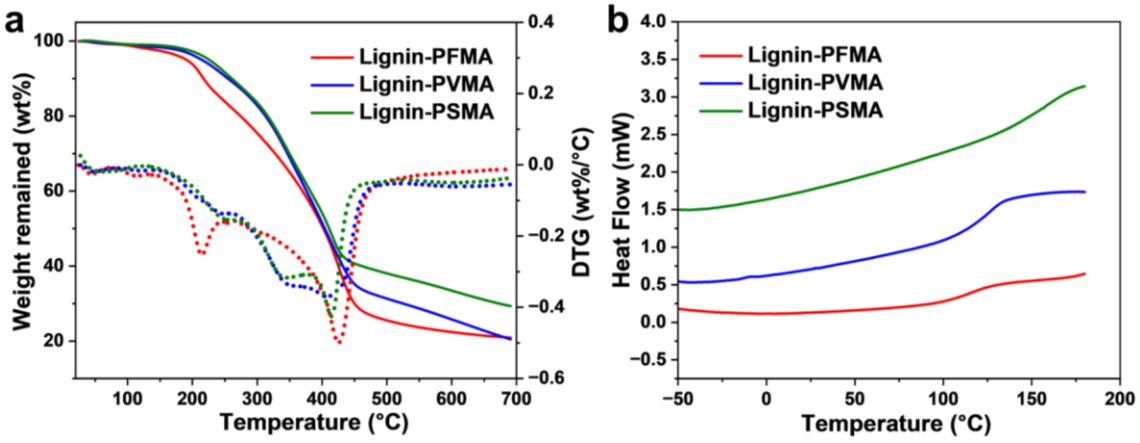

Figure 2. (a) TGA curves in a nitrogen atmosphere and (b) DSC curves of Lignin-PFMA, Lignin-PVMA, and Lignin-PSMA copolymers.

Table 1. The summary of thermal properties of lignin-based copolymers.

Sample Name	T_g (°C)	T_{d5} (°C)	Weight residue at 500 °C (wt%)	M_n (g/mol)[a]	*Dispersity (Đ)*
Lignin-PFMA	110.9	191.1	25.5	18,000	3.59
Lignin-PVMA	126.2	214.3	31.3	19,000	1.58
Lignin-PSMA	-	225.9	38.0	16,000	2.52

[a] THF-GPC value

3.2. Engineering lignin copolymers into nanobeads and nanofibers

After verifying the successful grafting of lignin, the resultant three kinds of lignin-based copolymers (Lignin-PFMA, Lignin-PVMA, and Lignin-PSMA) were engineered into nanobeads by solvent shifting via dialysis and nanofibers by electrospinning. Lignin nanobeads were prepared via a solvent-shifting method, where the solvent was slowly shifted from THF to DI water by dialysis. To obtain lignin-based nanobeads via dialysis, chemical modification of lignin is not mandatory, and there have been some works on extracted unmodified lignin [5, 24]. However, the variable chemical modification of lignin could expand the lignin-based nanobeads library because the chemically modified lignin shows different solubility in THF and the interaction with anti-solvent water compared to virgin lignin. This difference will induce a controllable change in the properties of the nanobeads. **Figure 3** and Table 2 show that nanobeads made from the Lignin-PSMA have a more uniform diameter distribution with an average PDI of 0.10 and an average diameter of 175.7 nm. From the SEM images of these three nanobeads, Lignin-PVMA ones clearly show a smaller diameter of 125.1 nm with a PDI of 0.15, and Lignin-PFMA nanobeads demonstrated the least homogeneous diameter distribution with a PDI of 0.16. Lignin-PFMA has an average diameter of 152.1 nm. It is assumed that the variations in polymer hydrophobicity, steric hindrance, and solubility in THF can lead to differing nucleation rates, which impact nanoparticle size. Lignin-PSMA, with its higher hydrophobicity, significant steric hindrance from two methoxy groups, and superior solubility in THF, experiences a slower nucleation rate, contributing to the formation of larger particles. Conversely, Lignin-PVMA, with moderate levels of these properties, results in the formation of smaller and less uniform particles. Lignin-PFMA, characterized by lower hydrophobicity, minimal steric hindrance (lacking

methoxy groups), and lower solubility in THF, would theoretically allow for tighter packing. However, as shown in Table 1, the high molecular weight polydispersity index (PDI) of 3.59 for Lignin-PFMA indicates a broad range of polymer chain lengths, leading to irregular aggregation and less efficient packing. This results in moderately sized particles due to the variability in chain lengths, which affects the overall particle size distribution (PDI: 0.16). The stability of lignin nanobeads was analyzed by measuring the size variation with time using DLS. All the lignin nanobeads showed stable dispersion and no significant deterioration within 112 days of monitoring, as presented in Figure 3. A reference sample, made from the lignin purchased from Sigma, was used for comparison, which shows a much smaller size of around 30 nm and good stability. Furthermore, no agglomerations of nanobeads were observed, which can be attributed to their highly negative charge, as shown in Table 2. Their zeta potentials are -34.23 mV for Lignin-PFMA, -32.67 mV for Lignin-PVMA, and -31.87 mV for Lignin-PSMA, respectively.

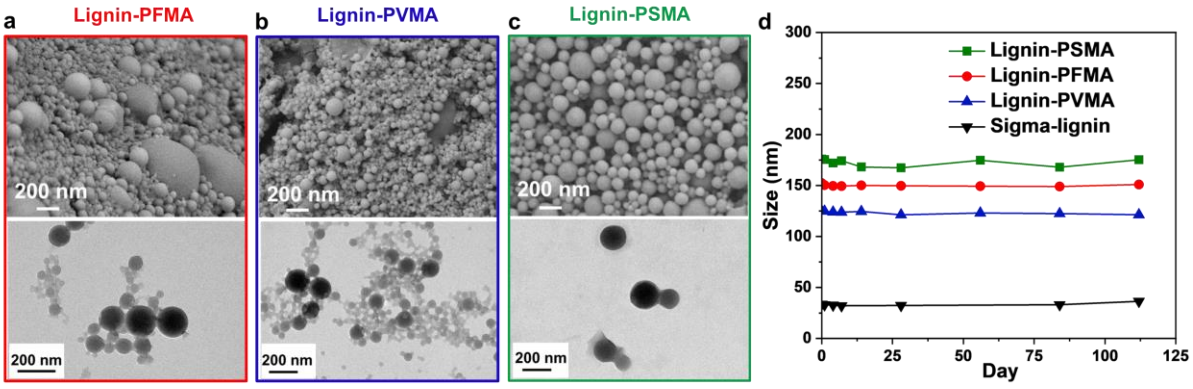

Figure 3. SEM and TEM images of lignin nanobeads from (a) Lignin-PFMA, (b) Lignin-PVMA, and (c) Lignin-PSMA. (d) The stability of lignin nanobeads analyzed by the diameter change within 112 days of monitoring.

Table 2. The summary of properties of lignin nanobeads via DLS analysis.

Sample Name	Average Size [nm]	PDI	Zeta potential [mV]
Lignin-PFMA	152.1±0.5	0.16	-34.23
Lignin-PVMA	125.1±0.5	0.15	-32.67
Lignin-PSMA	175.7±2.4	0.10	-31.87

Electrospinning is a simple and low-cost method to process lignin-based materials into nano- or micro-fibrous membranes [25, 26]. Successful electrospinning of lignin to produce nanofibers requires a homogeneous and suitable spinning solution with proper viscosity and electrical conductivity. Because of the intrinsic brittleness, pure lignin is not ideal for nanofibers by electrospinning. Therefore, for the electrospinning of lignin materials, the conventional process consists of first modifying lignin with the common polymers (PLA, PCL, and PHB) to lignin-based copolymers and then incorporating the lignin-based copolymers into the same or compatible polymer matrix, which overcame the intrinsic brittleness of lignin and facilitated the electrospinning process. Apparently, in these cases, lignin, despite its potential as a sustainable substitute for petrol-based synthetic polymers, is adopted in a limited amount as a filler within the polymer matrix, largely due to its poor processability in electrospinning. In our work, no such assisting polymers were adopted. Both Lignin-PFMA and Lignin-PSMA have good solubility in 1,1,1,3,3,3-hexafluoro-2-propanol (HFP). Therefore, 12 wt% HFP solutions were prepared. However, Lignin-PVMA showed difficulties when dissolving in HFP. Thus, only a 10 wt% solution was prepared for electrospinning, and the obtained fibrous membranes showed immense beads in the fibers. Lignin-PSMA displayed the best suitability for electrospinning among them but with a fiber diameter ranging from nano- to micro-size, 1110 ± 610 nm. Lignin-PFMA produced fibers with observed beading and broken fibers, with a similar diameter to Lignin-PSMA of 1180 ± 700 nm. Lignin-PVMA produces significantly thinner fibers of 310 ± 22 nm. The observed variations in nanofiber diameter may stem from differing solubility in the HFP solvent, impacting solution homogeneity during electrospinning. Solubility differences affect solution viscosity and surface tension, influencing polymer jet stretching and thinning, thus affecting fiber diameter uniformity.

The hydrophobicity of the obtained lignin nanofiber membranes was analyzed through water contact angle measurement, as shown in **Figure 4**. Lignin-PVMA nanofiber membranes showed the least hydrophobicity, with a contact angle of 84°. Nanofiber membranes made of Lignin-PFMA and Lignin-PSMA showed similar hydrophobicity with contact angles of 120° and 121°, respectively. The decreased hydrophobicity observed in Lignin-PVMA nanofiber membranes may be attributed to the smaller fiber diameter, which likely resulted in increased porosity. This increased porosity provides more pathways for

water infiltration and retention within the nanofiber structure, leading to higher hydrophilicity. In addition, smaller diameter nanofibers typically have a higher surface area-to-volume ratio compared to larger diameter nanofibers, allowing for enhanced interaction with water molecules and thus leading to more pronounced wetting behavior [27]. The presence of methoxy groups in the phenyl ring of the methacrylate monomers increases electron density, potentially decreasing hydrophobicity by enhancing polymer backbone polarity. However, the copolymer structure is unlikely to significantly affect hydrophobicity.

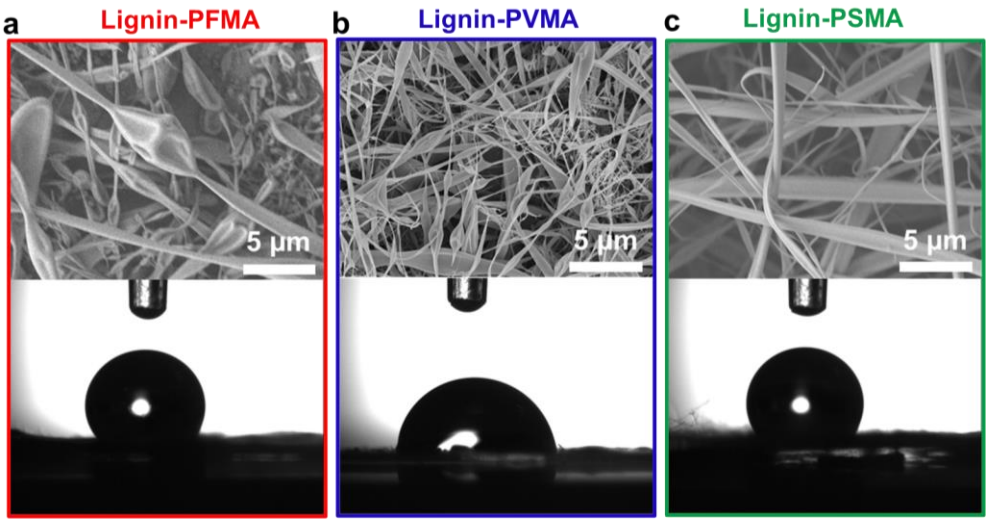

Figure 4. SEM images of lignin nanofibers. Water contact angles of nanofiber membranes. (a) Lignin-PFMA, (b) Lignin-PVMA, (c) Lignin-PSMA.

3.3. Cytotoxicity of lignin nanobeads and nanofibers

Two cell types, CCL9.1 and WS1, are used to evaluate the biocompatibility of the obtained lignin nanobeads and nanofibers. The cell viability results of lignin nanobeads are displayed in **Figure 5** (CCL9.1 cell) and **Figure 6** (WS1 cell). Overall, the use of lignin nanobeads for biomedical applications is promising, with all samples maintaining at least 80% cell viability in both cell types.

The biocompatibility of the polymers is affected by several factors, including cationic charge density, molecular weight, concentration, and hydrophilicity [28, 29]. In this study, the relatively high biocompatibility of lignin nanobeads may be partly accountable to their surface negative charges, which do

not destabilize the cell membrane. As shown in Figures 5a and 6a, CCL9.1 cells exhibited slightly higher viability compared to WS1 cells across all samples, with viability levels exceeding 90%. Notably, Lignin-PVMA achieved the highest viability, approaching 100% at all tested concentrations in CCL9.1 cells. A comparison reveals that Lignin-PSMA demonstrated the best biocompatibility with WS1 cells, whereas Lignin-PVMA resulted in the highest cell viability for CCL9.1 cells.

Despite growing interest in the use of lignin for biomaterial applications, limited research has focused on elucidating cell-lignin interactions. Our study aims to address this gap and contribute novel insights into this area. The observed biocompatibility of Lignin-PSMA may be attributed to its lower molecular weight, consistent with findings by Menima-Medzogo et al., who reported that fractionated low molecular weight lignin exhibited cytocompatibility with multiple cell types [30]. In contrast, the cytotoxicity often associated with high molecular weight polymers may stem from their potential to form permanent pores in cell membranes [31]. Meanwhile, the high cell viability of CCL9.1 cells exposed to Lignin-PVMA correlated with its highest hydrophilicity among the lignin nanobeads, reflecting previous findings that enhanced hydrophilicity of lignin composites improves cell viability [32-34]. Similarly, lignin nanoparticles that have been coated to increase hydrophilicity have also demonstrated high cell viability [35, 36]. Additionally, prior studies have reported that hydrophobic surfaces correlated with reduced cell adhesion, delayed cell cycle progression, and a higher number of apoptotic cells [37].

In contrast, commercially available Sigma-Aldrich lignin dissolved in methanol (referred to as Sigma-Lignin) showed more variable cytotoxicity. For CCL9.1 cells, viability decreased with increasing Sigma-Lignin concentration (**Figure 5**), suggesting concentration-dependent toxicity. However, concentrations below 0.05 mg/mL may still be suitable for biomedical use. For WS1 cells, there were no statistically significant differences in cell viability across Sigma-Lignin concentrations ($p > 0.05$; **Figure 6**), indicating limited compatibility regardless of concentration.

At equivalent concentrations, all lignin nanobead formulations exhibited significantly higher WS1 cell viability than Sigma-Lignin ($p < 0.05$, effect size $d > 1$). Similar observations were noted for the lignin nanobeads incubated with CCL9.1 cells at 0.1 mg/ml and 0.2 mg/ml ($p < 0.05$ and $d > 1$). These results

collectively support the conclusion that nanostructuring lignin into nanobeads significantly enhances its biocompatibility and widens its potential biomedical applications.

To further assess biocompatibility, cell morphology was examined via optical microscopy. The CCL9.1 cells appeared spherical, and some were spindle-shaped under normal culture conditions (Figure 5). The incubation with 0.05 mg/mL lignin and its nanobeads did not lead to a visible change in the morphology of the cells. Under normal culture, the WS1 cells developed an extensive network with the formation of tight junctions (Figure 6). The WS1 cells incubated with 0.05 mg/mL lignin nanobeads had the same observations. Regarding the incubation with Sigma-Lignin, the wells were too dark to detect any possible network that might have been available. These morphological assessments are consistent with the results from the cell viability assays. Future research may explore the development of drug delivery systems and UV-protective pharmaceutical formulations with light-sensitive components, leveraging the lignin-based nanobeads synthesized in this study.

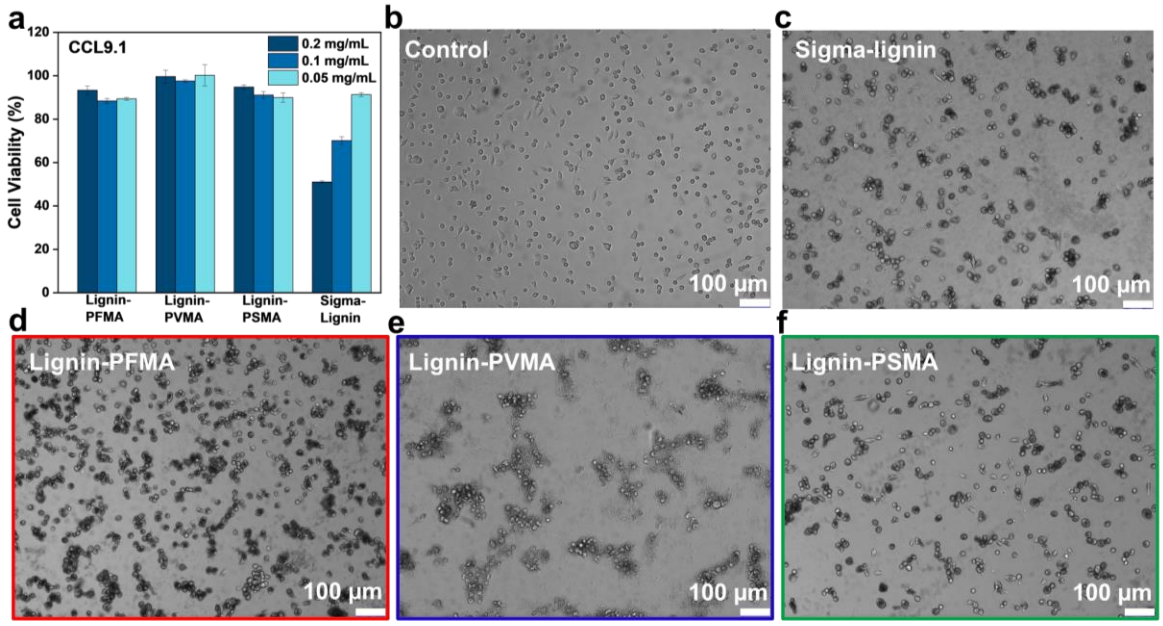

Figure 5. (a) Cytotoxicity of lignin nanobeads evaluated with CCL9.1 cells. SEM images of the CCL9.1 cells after 24 h of incubation (b) in a control state, (c) with the presence of lignin in methanol solution, (d) Lignin-PFMA, (e) Lignin-PVMA, and (f) Lignin-PSMA nanobeads.

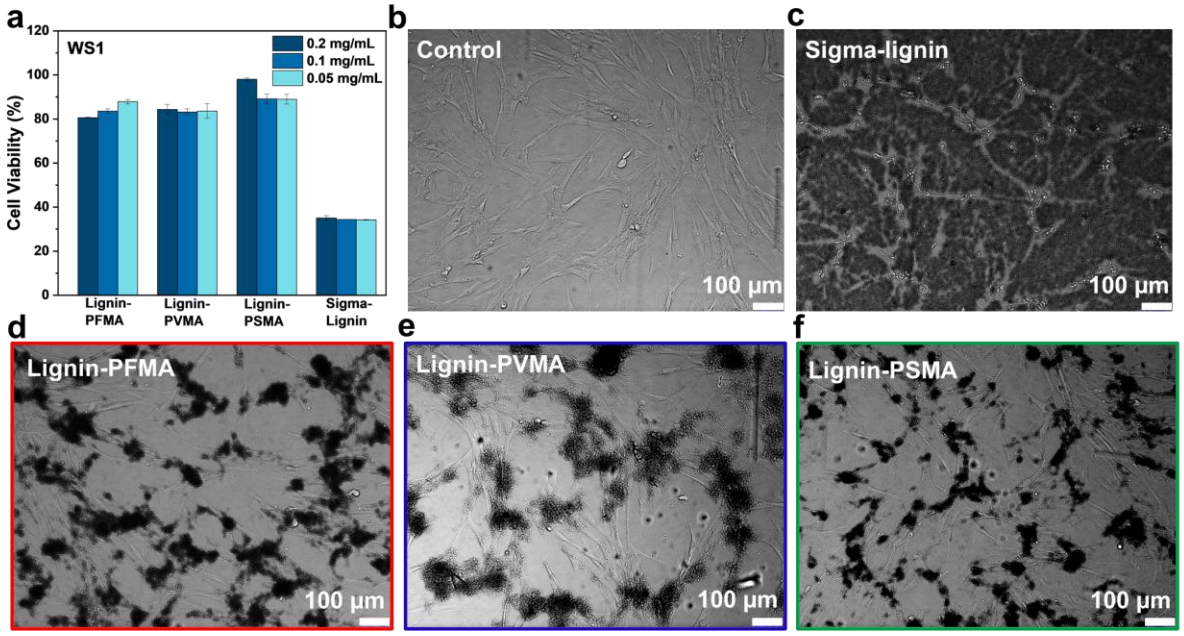

Figure 6. (a) Cytotoxicity of lignin nanobeads evaluated with WS1 cells. SEM images of the WS1 cells after 24 h of incubation (b) in a control state, (c) with the presence of lignin in methanol solution, (d) Lignin-PFMA, (e) Lignin-PVMA, and (f) Lignin-PSMA nanobeads.

The biocompatibility of lignin nanofibers was also evaluated. As shown in Figure 7, both CCL9.1 and WS1 cells maintained approximately 80% viability after 3 days of incubation with the nanofibers. Both types of lignin nanofibers seem to display similar biocompatibility with both cell types ($p > 0.05$). To further investigate, Lignin-PSMA was incubated with both cell types for 5 days. Cells appeared to be entangled within the nanofibers, and the extracellular matrix was detectable in CCL9.1 samples, supporting the biocompatibility of the Lignin-PSMA nanofibers. In contrast, the Lignin-PVMA nanofiber film produced by electrospinning is not intact and big enough for testing. Given their promising cell biocompatibility, the developed pure lignin-based nanofibers hold potential for future applications in wound dressings and tissue engineering scaffolds.

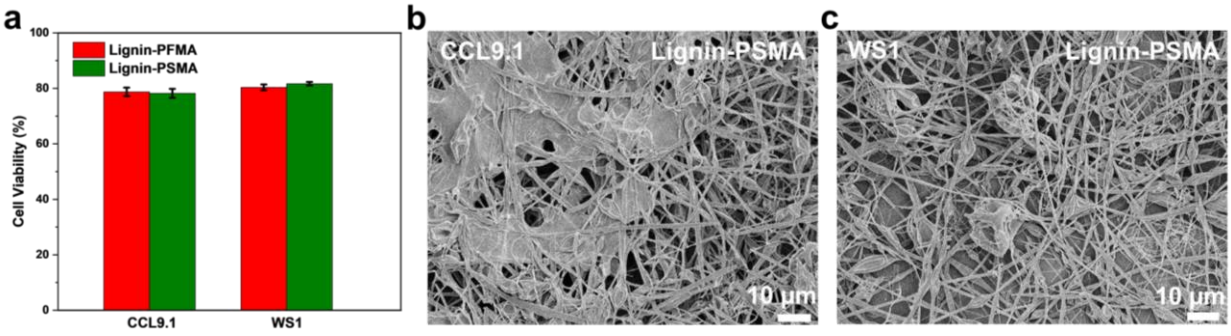

Figure 7. (a) Cytotoxicity of lignin nanofibers evaluated with CCL9.1 cells and WS1 cells. (b) and (c) SEM images of the cells after 5 days of incubation with Lignin-PSMA.

3.4. Potential applications of lignin nanobeads and nanofibers

As shown in Figure 8a, Lignin-PFMA copolymers showed superior antioxidant activity, as demonstrated by the DPPH radical scavenging assay. After 24 hours, an inhibition rate of 77.5% was recorded for Lignin-PFMA copolymers, compared to 63.3% for Lignin-PSMA (Figure S6a). The high radical scavenging capacity can be attributed to the polyaromatic structure and abundant phenolic groups inherent to native lignin. As shown in the schematic illustration in Figure S7, the phenolic hydroxyl groups act as effective hydrogen and electron donors, neutralizing free radicals by donating a hydrogen atom or an electron [38, 39]. Furthermore, the resulting phenoxyl radicals are stabilized through resonance delocalization across the aromatic ring, which reduces their reactivity and prevents propagation of oxidative damage. Additionally, the phenyl ring in PFMA and its conjugation with the lignin backbone likely contribute to enhanced radical stabilization. Lignin is well-known for its strong UV absorbance and excellent UV-shielding performance, attributed to its conjugated phenolic structures, particularly within the UVA (320-400 nm) and UVB (280-320 nm) ranges [40]. The UV absorption properties of lignin copolymers were evaluated both in lignin copolymer solutions (Figure 8b, Figure S6b) and when incorporated into tretinoin cream formulations (Figure 8c). All lignin copolymers exhibited strong UV absorption in the range of 280-320 nm, confirming their potential as effective UV-blocking agents.

Given the excellent bio-compatibility, antioxidant activities, and UV-blocking properties of synthesized lignin copolymers and their corresponding nanomaterials, several potential applications are proposed in Figure 8d, including lignin nanobeads for UV protection of light-sensitive components, drug delivery systems, lignin nanofibers for wound dressing and tissue engineering. Tretinoin cream, commonly used in dermatology for acne and melasma treatment, is very sensitive to light and loses effectiveness upon UV exposure. The tretinoin cream formulation containing lignin nanobeads showed higher absorbance across the entire tested wavelength range, indicating enhanced UV-blocking performance (Figure 8c), which will protect tretinoin cream from degradation when exposed to light. In the context of UV-protective pharmaceuticals, lignin can absorb UV radiation, thereby preventing it from reaching and degrading light-sensitive components. Additionally, the incorporation of lignin could inhibit the oxidative degradation of tretinoin due to the antioxidant properties, further enhancing its stability under UV light. Lignin nanobeads have the potential to encapsulate drugs and enable controlled and sustained drug release, owing to their antioxidant properties. These characteristics, combined with their UV-blocking performance, further support their potential use in light-sensitive drug delivery systems. In addition, the demonstrated antioxidant activities and bio-compatibility of lignin copolymers could also support their potential applications for wound dressing and tissue engineering, as illustrated in Figure 8d. Our previous work has demonstrated the feasibility of using lignin-copolymer nanofibers in tissue engineering applications [8, 11].

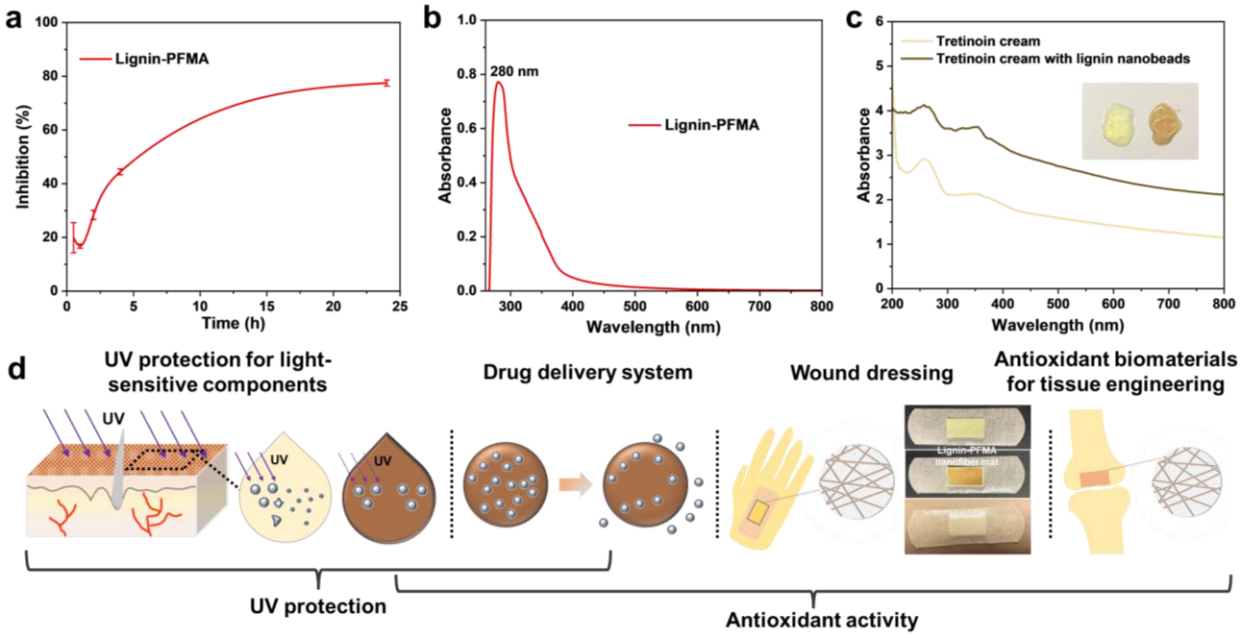

Figure 8. (a) Antioxidant properties of Lignin-PFMA copolymers. (b) UV-Vis absorbance of Lignin-PFMA copolymers. (c) UV-Vis absorbance of pristine tretinoin cream and tretinoin cream with lignin nanobeads (inserted photos of pristine cream and cream with lignin nanobeads). (d) Application exploitation and potential future application scenarios of developed lignin copolymer nanomaterials, including UV-protective pharmaceutical formulations with light-sensitive components, drug delivery systems, wound dressing, and antioxidant biomaterials for tissue engineering.

4. Conclusions

In this work, lignin was successfully grafted with three kinds of lignin-derived functional groups, namely, Lignin-PFMA, Lignin-PVMA, and Lignin-PSMA, by RAFT copolymerization. These three copolymers exhibit distinct features, reflecting differences in the steric hindrance and solubility. These variations in copolymer characteristics lead to varying sizes and properties of the obtained nanomaterials. This underscores the critical role of copolymer steric effects in determining its solubility behavior and interactions with solvents, subsequently affecting the properties of the obtained lignin-based nanomaterials. The lignin-*graft*-lignin copolymer nanobeads, made from solvent shifting via dialysis, showed stability in morphology within the observation duration of 112 days. The lignin-*graft*-lignin copolymer nanofibers

were successfully prepared without the need for other conventional polymers in electrospinning, using the copolymer as the sole feedstock. In addition, we found that engineering lignin by grafting with lignin derivatives and eventually designing it into nanobeads and nanofibers is a viable way to improve the biocompatibility of lignin materials, implying a broader range of applications in biomedical fields, such as UV-protection for light-sensitive components, controlled drug delivery systems, wound dressing, and antioxidant biomaterial scaffolds for tissue engineering.

Acknowledgments

This research is supported by the RIE2025 MTC Individual Research Grants (M22K2c0085), administered by the Agency of Science, Technology and Research (A*STAR), Singapore. This work was also supported by the National Medical Research Council (NMRC), Singapore, under its Clinician Scientist-Individual Research Grant (MOH-001357-00) and National Research Foundation (NRF) Singapore under its NRF Investigatorship (NRF-NRFI07–2021–0003).

Conflict of Interest

The authors declare no conflict of interest.

Author Contributions

T.W., S.S., and P.L.C. prepared the manuscript draft; D.K. reviewed and edited the manuscript. Conceptualization: D.K., X.J.L.; Methodology: T.W., S.S., P.L.C., and C.G.W.; Investigation: T.W., S.S., P.L.C., C.G.W., P.J.O., R.Y., and G.L.; Supervision: Q.Z., Z.L., X.J.L., and D.K.. All authors have read and agreed to the published version of the manuscript.

References

[1] A.J. Ragauskas, G.T. Beckham, M.J. Biddy, R. Chandra, F. Chen, M.F. Davis, B.H. Davison, R.A. Dixon, P. Gilna, M. Keller, P. Langan, A.K. Naskar, J.N. Saddler, T.J. Tschaplinski, G.A. Tuskan, C.E. Wyman, Lignin valorization: improving lignin processing in the biorefinery, Science 344(6185) (2014) 1246843.
[2] S. Sugiarto, Y. Leow, C.L. Tan, G. Wang, D. Kai, How far is Lignin from being a biomedical material?, Bioactive Materials 8 (2022) 71-94.

[3] B. Jiang, C. Chen, Z. Liang, S. He, Y. Kuang, J. Song, R. Mi, G. Chen, M. Jiao, L. Hu, Lignin as a Wood‐Inspired Binder Enabled Strong, Water Stable, and Biodegradable Paper for Plastic Replacement, Advanced Functional Materials 30(4) (2019).
[4] Q. Xia, C. Chen, Y. Yao, J. Li, S. He, Y. Zhou, T. Li, X. Pan, Y. Yao, L. Hu, A strong, biodegradable and recyclable lignocellulosic bioplastic, Nature Sustainability 4(7) (2021) 627-635.
[5] M. Lievonen, J.J. Valle-Delgado, M.-L. Mattinen, E.-L. Hult, K. Lintinen, M.A. Kostiainen, A. Paananen, G.R. Szilvay, H. Setälä, M. Österberg, A simple process for lignin nanoparticle preparation, Green Chemistry 18(5) (2016) 1416-1422.
[6] T. Sathasivam, L. Hu, S. Sugiarto, Q. Dou, Z. Zhang, H. Ru Tan, Y. Leow, Q. Zhu, C.L. Ken Lee, H.D. Yu, D. Kai, Facile Fabrication of Lignin-Cellulose Green Nanogels, Chemistry–An Asian Journal 17(21) (2022) e202200671.
[7] M.S. Alqahtani, A. Alqahtani, A. Al-Thabit, M. Roni, R. Syed, Novel lignin nanoparticles for oral drug delivery, Journal of Materials Chemistry B 7(28) (2019) 4461-4473.
[8] R. Liang, X. Yang, P.Y.M. Yew, S. Sugiarto, Q. Zhu, J. Zhao, X.J. Loh, L. Zheng, D. Kai, PLA-lignin nanofibers as antioxidant biomaterials for cartilage regeneration and osteoarthritis treatment, Journal of Nanobiotechnology 20(1) (2022) 327.
[9] D. Kai, W. Ren, L. Tian, P.L. Chee, Y. Liu, S. Ramakrishna, X.J. Loh, Engineering Poly(lactide)–Lignin Nanofibers with Antioxidant Activity for Biomedical Application, ACS Sustainable Chemistry & Engineering 4(10) (2016) 5268-5276.
[10] J. Wang, L. Tian, B. Luo, S. Ramakrishna, D. Kai, X.J. Loh, I.H. Yang, G.R. Deen, X. Mo, Engineering PCL/lignin nanofibers as an antioxidant scaffold for the growth of neuron and Schwann cell, Colloids Surf B Biointerfaces 169 (2018) 356-365.
[11] R. Liang, J. Zhao, B. Li, P. Cai, X.J. Loh, C. Xu, P. Chen, D. Kai, L. Zheng, Implantable and degradable antioxidant poly(epsilon-caprolactone)-lignin nanofiber membrane for effective osteoarthritis treatment, Biomaterials 230 (2020) 119601.
[12] P.L. Chee, P.Y.M. Yew, D. Kai, X.J. Loh, Reinforcement of aligned cellulose fibers by lignin-polyester copolymers, Materials Today Chemistry 18 (2020).
[13] S. Laurichesse, L. Avérous, Chemical modification of lignins: Towards biobased polymers, Progress in Polymer Science 39(7) (2014) 1266-1290.
[14] P. Figueiredo, K. Lintinen, J.T. Hirvonen, M.A. Kostiainen, H.A. Santos, Properties and chemical modifications of lignin: Towards lignin-based nanomaterials for biomedical applications, Progress in Materials Science 93 (2018) 233-269.
[15] I. Zaborniak, A. Macior, P. Chmielarz, M. Caceres Najarro, J. Iruthayaraj, Lignin-based thermoresponsive macromolecules via vitamin-induced metal-free ATRP, Polymer 219 (2021).
[16] S. Jiang, D. Kai, Q.Q. Dou, X.J. Loh, Multi-arm carriers composed of an antioxidant lignin core and poly(glycidyl methacrylate-co-poly(ethylene glycol)methacrylate) derivative arms for highly efficient gene delivery, Journal of Materials Chemistry B 3(34) (2015) 6897-6904.
[17] Y.S. Kim, J.F. Kadla, Preparation of a Thermoresponsive Lignin-Based Biomaterial through Atom Transfer Radical Polymerization, Biomacromolecules 11(4) (2010) 981-988.
[18] D. Khatri, S.B.B. Chhetri, Reducing Sugar, Total Phenolic Content, and Antioxidant Potential of Nepalese Plants, BioMed Research International 2020 (2020) 7296859.
[19] J. Dominguez-Robles, E. Larraneta, M.L. Fong, N.K. Martin, N.J. Irwin, P. Mutje, Q. Tarres, M. Delgado-Aguilar, Lignin/poly(butylene succinate) composites with antioxidant and antibacterial properties for potential biomedical applications, International Journal of Biological Macromolecules 145 (2020) 92-99.
[20] S. Gao, Z. Cheng, X. Zhou, Y. Liu, J. Wang, C. Wang, F. Chu, F. Xu, D. Zhang, Fabrication of lignin based renewable dynamic networks and its applications as self-healing, antifungal and conductive adhesives, Chemical Engineering Journal 394 (2020).
[21] S. Boner, K. Parkatzidis, N.D.A. Watuthanthrige, A. Anastasaki, RAFT polymerization of renewable monomers with dithiobenzoates: Effect of Z-group substituents and reaction conditions, European Polymer Journal 205 (2024) 112721.

[22] F.L. Hatton, Recent advances in RAFT polymerization of monomers derived from renewable resources, Polymer Chemistry 11(2) (2020) 220-229.
[23] H. Chung, A. Al-Khouja, N.R. Washburn, Lignin-Based Graft Copolymers <italic>via</italic> ATRP and Click Chemistry, Green Polymer Chemistry: Biocatalysis and Materials II, American Chemical Society2013, pp. 373-391.
[24] L. Matsakas, M. Gerber, L. Yu, U. Rova, P. Christakopoulos, Preparation of low carbon impact lignin nanoparticles with controllable size by using different strategies for particles recovery, Industrial Crops and Products 147 (2020) 112243.
[25] D. Kai, S. Jiang, Z.W. Low, X.J. Loh, Engineering highly stretchable lignin-based electrospun nanofibers for potential biomedical applications, Journal of Materials Chemistry B 3(30) (2015) 6194-6204.
[26] M. Kumar, M. Hietala, K. Oksman, Lignin-Based Electrospun Carbon Nanofibers, Frontiers in Materials 6 (2019).
[27] M.N. Pervez, M.E. Talukder, M.R. Mishu, A. Buonerba, P. Del Gaudio, G.K. Stylios, S.W. Hasan, Y. Zhao, Y. Cai, A. Figoli, T. Zarra, V. Belgiorno, H. Song, V. Naddeo, One-Step Fabrication of Novel Polyethersulfone-Based Composite Electrospun Nanofiber Membranes for Food Industry Wastewater Treatment, Membranes, 2022.
[28] H.A. Santos, J. Riikonen, J. Salonen, E. Makila, T. Heikkila, T. Laaksonen, L. Peltonen, V.P. Lehto, J. Hirvonen, In vitro cytotoxicity of porous silicon microparticles: effect of the particle concentration, surface chemistry and size, Acta Biomaterialia 6(7) (2010) 2721-31.
[29] D. Fischer, Youxin Li, Barbara Ahlemeyer, Josef Krieglstein, T. Kissel, In vitro cytotoxicity testing of polycations: influence of polymer structure on cell viability and hemolysis, Biomaterials 24(7) (2003) 1121-1131.
[30] J.A. Menima-Medzogo, K. Walz, J.C. Lauer, G. Sivasankarapillai, F.R. Gleuwitz, B. Rolauffs, M.-P. Laborie, M.L. Hart, Characterization and In Vitro Cytotoxicity Safety Screening of Fractionated Organosolv Lignin on Diverse Primary Human Cell Types Commonly Used in Tissue Engineering, Biology 11(5) (2022) 696.
[31] B.D. Monnery, M. Wright, R. Cavill, R. Hoogenboom, S. Shaunak, J.H.G. Steinke, M. Thanou, Cytotoxicity of polycations: Relationship of molecular weight and the hydrolytic theory of the mechanism of toxicity, International Journal of Pharmaceutics 521(1-2) (2017) 249-258.
[32] A. Bužarovska, J. Blazevska-Gilev, B.T. Pérez-Martnez, L.R. Balahura, G.G. Pircalabioru, S. Dinescu, M. Costache, Poly(l-lactic acid)/alkali lignin composites: properties, biocompatibility, cytotoxicity and antimicrobial behavior, Journal of Materials Science 56(24) (2021) 13785-13800.
[33] S. Amini, A. Saudi, N. Amirpour, M. Jahromi, S.S. Najafabadi, M. Kazemi, M. Rafienia, H. Salehi, Application of electrospun polycaprolactone fibers embedding lignin nanoparticle for peripheral nerve regeneration: In vitro and in vivo study, International Journal of Biological Macromolecules 159 (2020) 154-173.
[34] A. Saudi, S. Amini, N. Amirpour, M. Kazemi, A. Zargar Kharazi, H. Salehi, M. Rafienia, Promoting neural cell proliferation and differentiation by incorporating lignin into electrospun poly(vinyl alcohol) and poly(glycerol sebacate) fibers, Materials Science and Engineering: C 104 (2019) 110005.
[35] R. Liu, T. Ding, P. Deng, X. Yan, F. Xiong, J. Chen, Z. Wu, Structure and properties of nanoparticles: DES-lignin-g-PNVCL coated aspirin by self-assembly, Biomaterials Science 10(15) (2022) 4284-4292.
[36] L. Siddiqui, N. Hasan, P.K. Mishra, N. Gupta, A.T. Singh, A. Madaan, M. Jaggi, S. Saad, A. Ekielski, Z. Iqbal, P. Kesharwani, S. Talegaonkar, CD44 mediated colon cancer targeting mutlifaceted lignin nanoparticles: Synthesis, in vitro characterization and in vivo efficacy studies, International Journal of Pharmaceutics 643 (2023) 123270.
[37] E.J. Chang, H.H. Kim, J.E. Huh, I.A. Kim, J. Seung Ko, C.P. Chung, H.M. Kim, Low proliferation and high apoptosis of osteoblastic cells on hydrophobic surface are associated with defective Ras signaling, Experimental Cell Research 303(1) (2005) 197-206.
[38] H. Sadeghifar, A.J. Ragauskas, Lignin as a Natural Antioxidant: Chemistry and Applications, Macromol 5(1) (2025).

[39] K. Li, W. Zhong, P. Li, J. Ren, K. Jiang, W. Wu, Recent advances in lignin antioxidant: Antioxidant mechanism, evaluation methods, influence factors and various applications, International Journal of Biological Macromolecules 251 (2023) 125992.
[40] Y. Zhang, M. Naebe, Lignin: A Review on Structure, Properties, and Applications as a Light-Colored UV Absorber, ACS Sustainable Chemistry & Engineering 9(4) (2021) 1427-1442.

Graphical abstract